Wide-field performance gradient at a mid-latitude site and at Dome C

Jeff Stoesz[a], Elena Masciadri[a], Susanna Hagelin[a,b] and Franck Lascaux[a]

[a]Osservatorio Astrofisico di Arcetri, Largo Enrico Fermi 5, 50125 Firenze, Italy;
[b]Uppsala Universitet, Department of Earth Sciences, Villavägen 16, S-752 36 Uppsala, Sweden

ABSTRACT

Dome C is considered a site particularly suited for wide-field imaging thanks to its shallow surface turbulent layer and its weak turbulence in the free atmosphere. What is the quantitative gain one can hope to achieve at Dome C with respect to a mid-latitude site? With the point spread function model defined analytically in the spatial frequency domain we are better able to connect the morphological and statistical behaviour of the turbulence profile to the trade-off between the adaptive telescope's field of view and a figure of merit for survey rate. A familiar image quality figure of merit is the radius of 50% encircled energy, and for J-band images it quickly identifies the requirement that will make a Dome C telescope, 8 meters above the ice, competitive with a mid-latitude one. From the radius of 50% encircled energy we derive the wide-field survey rate equation to estimate the impact of uncertainty in the vertical distribution of ground-layer turbulence on the trade-off between field of view (in the domain 10-20 arcminutes) and their survey rate.

Keywords: turbulence, adaptive optics, site testing, astronomical surveys.

1. INTRODUCTION

The astronomical incentives for building a steerable optical/near-infrared telescope at Dome C, on the Antarctic plateau include: lower background light, low surface wind speeds, and much less turbulence above the surface-layer (few tens of meters above the ice). Some of the proposed telescopes for Dome C will have either mid-infrared or a modest aperture to achieve diffraction-limited performance that is much better than similar telescopes at mid-latitudes. For a 10-meter or even a 2-meter class optical/NIR telescope proposed for Dome C, a ground-layer adaptive optics (GLAO) system will correct the surface-layer turbulence.

Accurate measurement of vertical distribution of the turbulence is unfortunately a factor in predicting the performance of adaptive telescopes as a function of the diameter of the field of view. There are several measurement techniques being advanced to provide statistics on the vertical distribution of the structure function coefficient, $C_n^2(h)$, and by end of this paper we will also quantify the impact of a potential uncertainty in the vertical distribution from Scidar and MASS measurements.

We will define scenarios for the vertical distribution of the turbulence based on the profile measurements at Dome C and our typical mid-latitude observatory site, the Vatican Advanced Technology Telescope (VATT) at Mt. Graham (32.7 N, 109.87 W, 3200 meters). The turbulence above the VATT is measured with Scidar[1] mounted on the telescope, which is about 10 meters above the ground and at the height of the tree tops. The Dome C (75.1 S, 123.3 E, 3260 meters) scenario will be based on MASS and SODAR measurements by [2] and balloon measurements by [3].

In Sec. 2 we describe how we will compute the radius of 50% encircled energy from the atmospheric scenarios. Then in Sec. 3 we describe how the scenarios are made from the measurement data. The survey rate as a function of field of view is discussed in Sec. 4.

Further author information: (Send correspondence to J.S.)
J.S.: E-mail: stoesz@arcetri.astro.it, Telephone: +39 055 2752 202

Ground-based and Airborne Telescopes II, edited by Larry M. Stepp, Roberto Gilmozzi,
Proc. of SPIE Vol. 7012, 70124C, (2008) · 0277-786X/08/$18 · doi: 10.1117/12.789639

2. PSF MODEL

The point spread function (PSF) figure of merit that is of particular importance to wide field astronomy is the radius of 50% encircled energy, computed at several points in the contiguous field of view and then averaged. The field average of this will be symbolized as $EE50$ here. We will compute $EE50$ starting with an analytically defined phase Power Spectral Density (PSD) for anisoplanatism and fitting error using theory presented in [4, 5]. Table 1 lists the model parameters selected here. Computation from the analytic phase PSD is a fast method to discover the performance gradient of $EE50$ as a function of θ, the diameter of the field of view.

Table 1. The parameters and assumptions of the GLAO PSF model.

phase PSD	von Kármán, $L_o = 30$ meters
telescope diameter	$D = 8$ meters
Deformable Mirror	square grid of actuators with pitch = Δ
Deformable Mirror	each actuator has a sinc-like influence function
Deformable Mirror	conjugated to height = 0
Wavefront Reconstruction	a wavefront with sampling Δ from each beacon
DM Command	the average of wavefront from the beacons
Beacons	4 point sources at range $H = 90$ km at zenith
Beacons	evenly distributed on a circle of diameter θ in the field
PSF locations	in a square field of view, the vertices intersect the circle between beacons
image wavelength	$\lambda = 1.25\mu m$

The impact of uncertainty in the height of turbulence depends on the basic GLAO system parameters, namely the diameter of the guide star asterism, θ, and the pitch that is controlled by the ground conjugated deformable mirror, Δ. The ratio $\Delta/\theta = h_{GZ}$ defines the height below which any contribution of turbulence to anisoplanatism wavefront error is negligible. The term grey-zone (GZ) was coined[5] to identify the heights above h_{GZ}, where the contribution to anisoplanatism is not negligible (also known as partially corrected zone).*

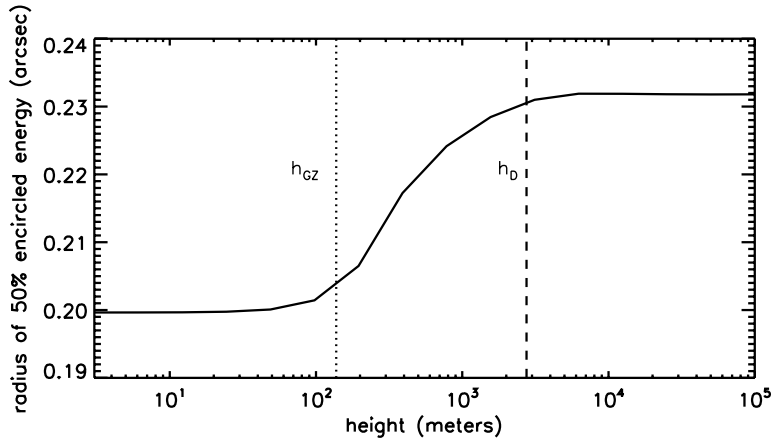

Figure 1. The grey-zone begins above h_{GZ}.

Fig. 1 helps illustrate this transition in the grey-zone, in terms of performance in the focal plane. The plot shows the $EE50$ figure of merit as a function of the height of one layer of turbulence added to a typical, smooth profile. Fig. 1 shows on a semi-log plot how the largest performance gradient, is at heights just above h_{GZ}. Note that the semi-log plot diminishes the steepness of the gradient. The gradient vanishes above $h_D = D/\theta$, where D is the telescope diameter.

In the following sections we will re-compute $EE50(\theta)$ with estimated uncertainty in the proportion of turbulence located at heights above or below h_{GZ}.

*See the approximate error transfer function in equation (8) and fig. 1 of [5] for further explanation.

3. MT. GRAHAM AND DOME C SCENARIOS

The Mt. Graham Scidarmeasurements include 851 with a wide binary to sample the ground-layer and 9911 that sample the free-atmosphere. Both have been reduced by [1] using the standard analysis of autocorrelation images to compute discretized turbulence strength J_i at height h_i. The J_i is related to $C_n^2(h)$ by

$$J_i = \int_{h_{b\,i}}^{h_{b\,i+1}} dh\ C_n^2(h). \tag{1}$$

The vertical resolution of the standard analysis of Scidar autocorrelation data in our ground-layer analysis here is about 120 meters and there is evidence provided in [6, 7] which suggest that the autocorrelation analysis alone may not be resolving a thinner surface-layer at Mt. Graham. It stands to reason that Mt. Graham may be better for wide field imaging than is presented here. In Sec. 3.1 we will describe how the ground-layer and free-atmosphere are reduced to form a composite statistical model.

The measurements we will use for Dome C are 1701 MASS+SODAR profile monitoring measurements by [2] during the Antarctic winter of 2004. Between 30 and 100 meters these data sample only two grid points and do not sample any turbulence below 30 meters. We complement that measurement campaign with the balloon-borne micro-thermal measurements of [3], which we use to estimate the exponential model parameters: scale height, h_A, and maximum strength, A.

$$C_n^2(h) = Ae^{(-h/h_A)}. \tag{2}$$

Using Eqn.(1) we get

$$J_i = -Ah_A\left(e^{(-h_{b\,i+1}/h_A)} - e^{(-h_{b\,i}/h_A)}\right). \tag{3}$$

We will choose the boundaries h_{bi} in Sec. 3.1. Using a average, weighted by $C_n^2(h)$

$$\begin{aligned} h_i = & \frac{\int_{h_{b\,i}}^{h_{b\,i+1}} dh\ C_n^2(h)\ h}{\int_{h_{b\,i}}^{h_{b\,i+1}} dh\ C_n^2(h)}. \\ = & \frac{-Ah_A\left[(h_{b\,i+1}+h_A)e^{(-h_{b\,i+1}/h_A)} - (h_{b\,i}+h_A)e^{(-h_{b\,i}/h_A)}\right]}{J_i}. \end{aligned} \tag{4}$$

We populate a lognormal distribution of values for the Dome C scale height, h_A, while $A = 740. \times 10^{-16}$ is fixed. A lognormal distribution of the scale height was created and has a median, first and last quartile of $h_A = [14, 9, 22]$ meters respectively. The corresponding lognormal distribution of seeing values has a median, first and last quartile values of [1.3, 0.98, 1.7] arcseconds. This distribution of seeing resembles the measurements from 8.5 meters above the ice in Table 1. of [3] (see also their updated results in [8]). The mean surface-layer profile from our synthetic distribution also resembles a telescope at about 8 meters above the ice in the mean C_n^2 profile of Fig. 1 in [3].

We use this model to define the grid points for the surface layer, up to 200 meters height. The turbulence measurements recorded by SODAR in the data of [2] we will attribute to a slab concentrated at 250 meters between the modelled surface-layer and the lowest MASS measurement, at 500 meters.

The data for the Mt. Graham (MG) scenario has weaker overall seeing (0.74 arcsecond median) than Dome C (DC, 1.2 arcsecond median). To illustrate the differences in the vertical distributions for these two sites we reduce the data to cumulative histograms of seeing in three slabs, shown in Fig. 2. The Dome C free atmosphere (right panel) and even upper ground-layer slab (middle)are quite calm. The DC scenario clearly has most turbulence concentrated between the telescope and 30 meters range (left panel Fig. 2). Remember our chosen exponential parameters are meant to correspond to 8 and 38 meters above the ice in the average profile Fig. 1 in [3].

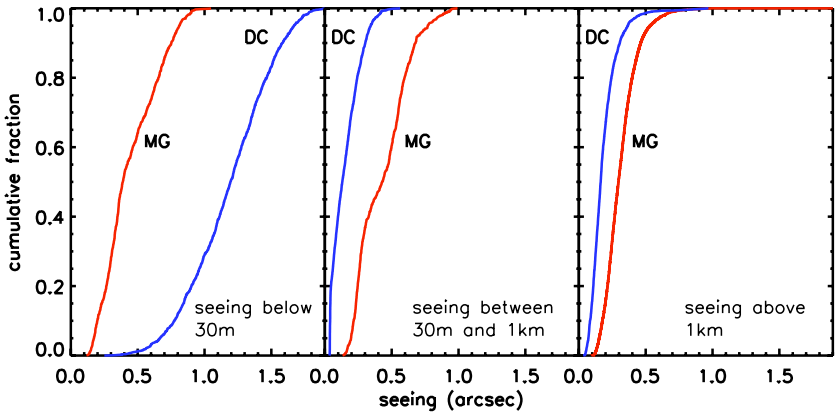

Figure 2. Comparison of the Dome C (DC) and Mt. Graham (MG) turbulence profile data used here, shown in terms of seeing in the critical layers. Heights given in the legend are heights above the telescope, not the ice or below the trees.

3.1 Reduction to composite profiles

We will reduce the number of PSFs that we have to calculate by reducing the profiles to composite statistical profiles of the ground-layer and free-atmosphere. Here we define the ground-layer to be between the site and 1000 meters above. The free-atmosphere is above 1000 meters. Since the measurements of the ground-layer and free-atmosphere at these sites is not simultaneous, we must create composite profiles that would closely reproduce the PSF statistics as though we had computed them on a full set of $J_i(h_i)$ data, uninterrupted in h and sampled at the same time. To do this we sort and combine the profiles of as described in [9] using the assumption of uncorrelated ground-layer and free-atmosphere seeing. We will briefly re-describe the process here in the context of our data.

Three groups of profiles in the ground-layer are identified using the sum of J_i. The first group are those profiles between the 20^{th} and 30^{th} percentile are combined in a simple average for J_i. We call them the "good" case. The 45^{th} to 55^{th} and 70^{th} to 80^{th} percentile profiles are combined similarly and called "typical" and "bad". In each group the grid of h_i is identical and hence remains unchanged by the combining process. The same process is done for the free-atmosphere. The result is a reduction to three ground layer profiles and three free-atmosphere profiles, which together have nine combinations for composite profiles that can reproduce the PSF statistics as though we had computed them on all of the $J_i(h_i)$ data.

3.1.1 Resampling the Composite Profiles for the PSF model

We want the PSF results to represent smooth continuous $C_n^2(h)$ profiles. In the next section we give PSF results from rebinned profiles with a sufficient number of grid points in the grey-zone, numerous enough such that the PSF figure of merit no longer changes with the number of grid points. This is simple to do for the ground-layer of Dome C because we can quickly redefine the h_b grid and re-calculate $J_i(h_i)$ with Eqn.(3) and Eqn.(4). For the measurements of Mt. Graham and the free-atmosphere of Dome C we divide several measured $J_i(h_i)$ grid into more numerous $J_j(h_j)$ using linear interpolation of the original discretized $C_n^2(h)$ data.

4. PREDICTED GLAO PERFORMANCE

The reduced composite $C_n^2(h)$ profiles for each site are are put into the PSF model then field averaged radius of 50% encircled energy of PSFs at a wavelength of $1.25\mu m$ are output. We plot a grid of nine sets of curves in Fig. 3 to illustrate differences between the deformable mirror pitch demanded by the two sites (rows) as well as the impact on GLAO performance by potential uncertainty in the measured vertical distribution of the turbulence strength (columns). The left and right columns of plots in Fig. 3 will be discussed in Sec. 4.1.

Let us first consider the central column of plots to identify the fundamental differences between weak and strong free-atmosphere sites. Mt. Graham are the red lines (grey if printed in black and white) and Dome C is

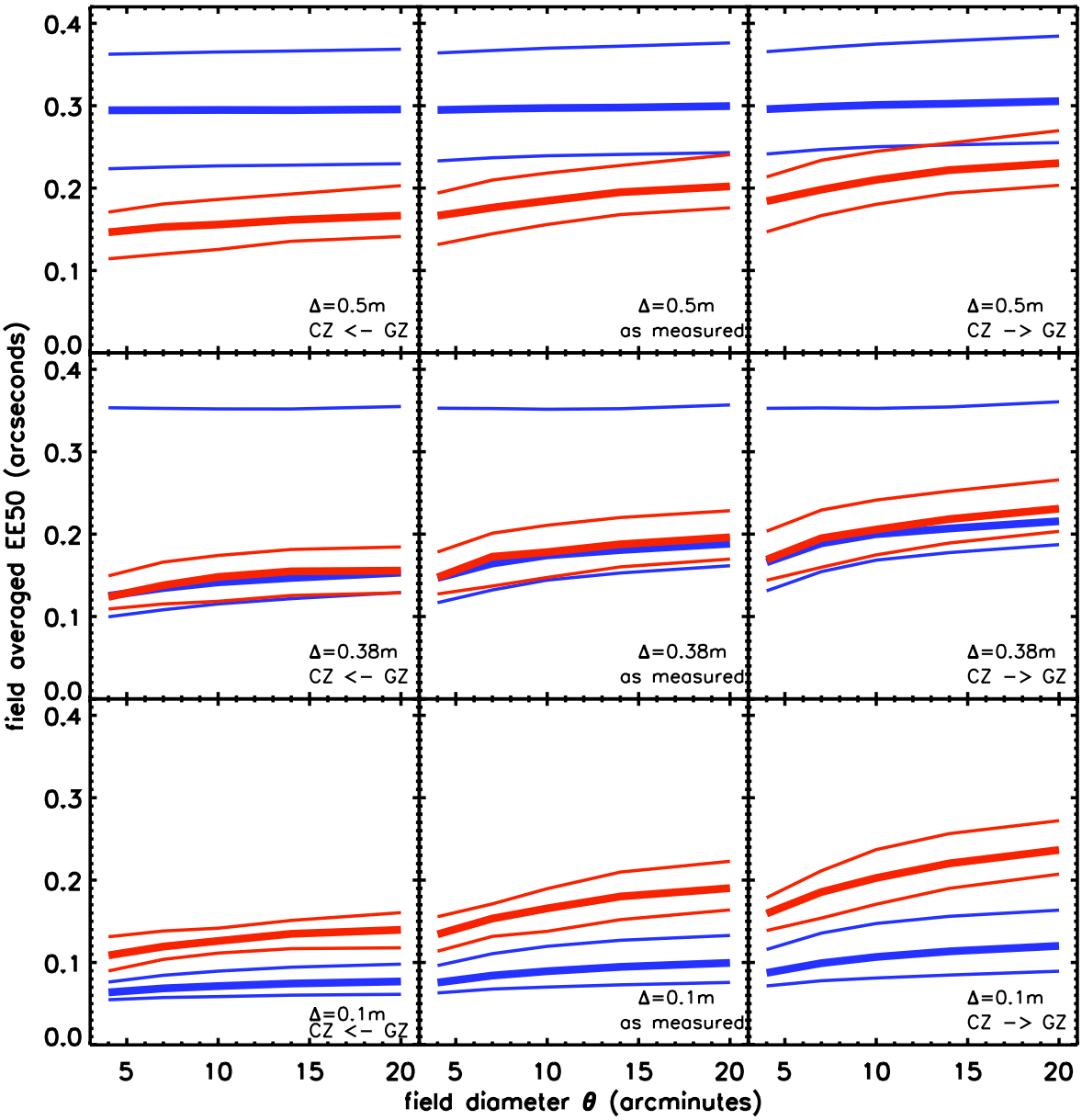

Figure 3. The field averaged radius of 50% encircled energy on PSFs with $\lambda = 1.25\mu m$, plotted as a function of the GLAO field of view. The three plots in each row of plots has the same actuator pitch, while each column has the same redistribution of the input composite profiles. Mt. Graham are the red lines (grey if printed in black and white) and Dome C is blue (or black).

blue (or black). The thicker lines are the median values while the thinner ones are the first and last quartiles of the distribution of $EE50$ values. In the upper plot of the central column, Mt. Graham $EE50$ gracefully increases with θ, as the bottom of the grey-zone (Sec. 2) reaches down into the surface-layer turbulence 100 to 250 meters thick. For this top middle panel the actuator pitch of the deformable mirror was $\Delta = 0.5$ meters and is grossly inadequate for J-band images in the Dome C scenario. The $EE50$ is not dependent on anisoplanatism of the correction because fitting error dominates.

In the central panel the pitch is $\Delta = 0.38$ meters, which improves correction at Mt. Graham slightly in

all conditions, and greatly improves Dome C for median or better conditions. The bottom plot shows the real potential for Dome C when the wavefront is controlled at a pitch of $\Delta = 0.1$ meters. There are of course other sources of wavefront error that should be included to make a realistic simulation for Dome C with $\Delta = 0.1$, but we can definitely say that the Dome C scenario requires a small pitch to be competitive. It is sometimes near the diffraction-limited $EE50$ with $\Delta = 0.1$. Mt. Graham on the other hand has more high altitude turbulence and is always limited by anisoplanatism for these values of Δ.

In the next subsection we will consider the columns of panels to the left and right of Fig. 3. They show how the field of view trade-off would differ if the measured vertical distribution has uncertainty.

4.1 Predicted performance gradient and the field of view trade-off

In addition to the initial cost of construction there is also the cost of the time required to complete the survey. Let us consider the slope of the function $EE50$ versus θ (field of view), and how our uncertainty in slope affects the field of view trade-off. It will help if we connect $EE50$ to the time required to complete an imaging survey.

When the PSF shape is smooth and broad, like a seeing-limited image. The radius of 50% encircled energy $EE50$ is quite closely related to the optimal photometry aperture, r, when the noise is dominated by the background light. For our GLAO correction of J-band images in fields of view from 10 to 20 arcminutes this condition is satisfied when there is more than about 0.5 arcseconds of seeing (V-band) above 30 meters from the deformable mirror conjugation. Fig. 2 shows that this is the case for Mt Graham more than half the time. In these conditions

$$r \simeq EE50. \tag{5}$$

The radius of the photometry aperture, r, is then related to the integration time, t, to achieve some signal to noise ratio for background-limited photometry at some magnitude by

$$\mathrm{SNR} = \frac{St}{\sqrt{b\pi r^2 t}} \tag{6}$$

Where S times t is the number of signal photons and $(b\pi r^2 t)$ is the number of background photons. Note also that to be background-limited the stellar fields must not be crowded, i.e. PSFs that do not severely overlap. In this situation

$$t \propto EE50^2. \tag{7}$$

The performance of a wide field survey telescope can be expressed as a survey rate, using the number of square arcminutes of sky that can be imaged to some limiting magnitude per unit time. Using the relationship in (7) for the field averaged radius of 50% encircled energy, we write the survey rate

$$R(\theta) \propto \frac{\theta^2}{EE50(\theta)^2}. \tag{8}$$

Scidar measurements produce faithful total integrals of turbulence, however, the vertical distribution may be uncertain.[10] We use a simple scheme to realize two alternate sets of scenarios, in the columns to the left and right. The left column of plots in Fig. 3 were computed from the $J_i(h_i)$ multiplied by 0.5 in the domain $h_{gz} < h_i < 6$ km, with the balance conserved by putting turbulence in the lowest layer, below h_{GZ}, into the corrected zone (CZ). Likewise the right column of plots is $J_i(h_i)$ multiplied by 1.5 in the domain $h_{gz} < h_i < 6$ km, with the balance conserved by removing turbulence from the lowest layer.

Let us now consider the trade-off between a 10 arcminute and a 20 arcminute field of view with uncertainty in the vertical distribution. From the middle row of plots, and from the median curves for Mt. Graham (thick red lines), the $EE50(10) = [0.150, 0.180, 0.205]$ in the [left, middle, and right] plots. Likewise $EE50(20) = [0.155, 0.195, 0.230]$. Using Eqn.(8) we get $R(20)/R(10) = [3.7, 3.4, 3.2]$. Which means that building a 20 arcminute adaptive telescope versus one with 10 arcminutes is expected to be 3.4 times faster survey, but it might be 3.7 or perhaps only 3.2 times faster. It is now easy to play with costs to see for oneself if this uncertainty is significant.

Suppose the start-up cost of the 20 arcminute telescope is $X(20)$ dollars and the 10 arcminute design is less expensive at $X(10)$ dollars. The operational budget of the survey is Y dollars to achieve the science goal over the

lifetime of the survey. The increased operational cost by switching to the 10 arcminute design is $Y \times R(20)/R(10)$, which would need to be less than $(X(20) - X(10))$ to be the cost effective choice for the Mt Graham scenario. With the uncertainty, the spread in values for the relative survey rate $R(20)/R(10)$, and therefore also the operational budget increase, is 15%.

5. CONCLUSIONS

The Dome C scenario, because of the high concentration of turbulence in the surface-layer, demands more actuators on the deformable mirror in order to be competitive with a telescope at a good mid-latitude site. Alternatively, the pier for the Dome C site could also made higher than the 8-meter pier we have modelled here. When the surface-layer is overcome, Dome C offers a wider corrected field of view.

We have used 50% uncertainty in the proportion of turbulence strength between the corrected-zone and the grey-zone (above h_{GZ} and below 6 km). This uncertainty can represent not just uncertainty in the site monitoring profiler(s), but it can also represent an inadequate number of samples in the profile statistics. In any case 50% is not a gross over estimate and its impact on the survey rate for a background-limited imaging survey was 15%.

An important future study using analytically defined phase power spectral density with turbulence profile statistics is a study of the non-uniformity of the radius of 50% encircled energy in the field, in addition to the field average. The morphology of the profile at the bottom of the grey-zone imposes trends on the PSF morphology and will combine with the field average in the performance gradient with θ, not just on $EE50(\theta)$ for background-limited stellar photometry, but other figures of merit connected to other types of science.

ACKNOWLEDGMENTS

This work is funded by a Marie Curie Excellence Grant (FOROT) MEXT-CT-2005-023878, FP6 Program. We thank John Storey's team for providing their Dome C MASS and SODAR data.

REFERENCES

1. S. E. Egner, E. Masciadri, and D. McKenna, "Generalized SCIDAR Measurements at Mount Graham," *PASP* **119**, pp. 669–686, June 2007.
2. J. S. Lawrence, M. C. B. Ashley, A. Tokovinin, and T. Travouillon, "Exceptional astronomical seeing conditions above Dome C in Antarctica," *Nature* **431**, pp. 278–281, Sept. 2004.
3. A. Agabi, E. Aristidi, M. Azouit, E. Fossat, F. Martin, T. Sadibekova, J. Vernin, and A. Ziad, "First Whole Atmosphere Nighttime Seeing Measurements at Dome C, Antarctica," *PASP* **118**, pp. 344–348, Feb. 2006.
4. L. Jolissaint, J.-P. Véran, and R. Conan, "Analytical modeling of adaptive optics: foundations of the phase spatial power spectrum approach," *Journal of the Optical Society of America A* **23**, pp. 382–394, Feb. 2006.
5. A. Tokovinin, "Seeing Improvement with Ground-Layer Adaptive Optics," *PASP* **116**, pp. 941–951, Oct. 2004.
6. S. E. Egner and E. Masciadri, "A G-SCIDAR for Ground-Layer Turbulence Measurements at High Vertical Resolution," *PASP* **119**, pp. 1441–1448, Dec. 2007.
7. J. Stoesz, E. Masciadri, S. Egner, S. Hagelin, and F. Lascaux, "Optical turbulence measurements with a generalized scidar at mt. graham for standard and high vertical resolution," in *these SPIE proceedings*, **7012**, 2008.
8. H. Trinquet, A. Agabi, J. Vernin, M. Azouit, E. Aristidi, and E. Fossat, "Nighttime Optical Turbulence Vertical Structure above Dome C in Antarctica," *PASP* **120**, pp. 203–211, Feb. 2008.
9. A. Tokovinin and T. Travouillon, "Model of optical turbulence profile at Cerro Pachón," *MNRAS* **365**, pp. 1235–1242, Feb. 2006.
10. A. Tokovinin, J. Vernin, A. Ziad, and M. Chun, "Optical Turbulence Profiles at Mauna Kea Measured by MASS and SCIDAR," *PASP* **117**, pp. 395–400, Apr. 2005.